ELSEVIER

Deep-Sea Research II 50 (2003) 3199–3221

DEEP-SEA RESEARCH
PART II

www.elsevier.com/locate/dsr2

Production regimes in four Eastern Boundary Current systems

Mary-Elena Carr[a,*], Edward J. Kearns[b]

[a] *Jet Propulsion Laboratory, California Institute of Technology, MS 300-323, 4800 Oak Grove, Pasadena, CA 91109-8099, USA*
[b] *Rosenstiel School of Marine and Atmospheric Science, University of Miami, 4600 Rickenbacker Causeway, Miami, FL 33149, USA*

Received 4 June 2002; received in revised form 23 June 2003; accepted 15 July 2003

Abstract

High productivity (maxima ~ 3 g C m^{-2} day^{-1}) of the Eastern Boundary Currents (EBCs), i.e. the California, Peru-Humboldt, Canary and Benguela Currents, is driven by a combination of local forcing and large-scale circulation. The characteristics of the deep water brought to the surface by upwelling favorable winds depend on the large-scale circulation patterns. Here we use a new hydrographic and nutrient climatology together with satellite measurements of the wind vector, sea-surface temperature (SST), chlorophyll concentration, and primary production modeled from ocean color to quantify the meridional and seasonal patterns of upwelling dynamics and biological response. The unprecedented combination of data sets allows us to describe objectively the variability for small regions within each current and to characterize the governing factors for biological production. The temporal and spatial environmental variability was due in most regions to large-scale circulation, alone or in combination with offshore transport (local forcing). The observed meridional and seasonal patterns of biomass and primary production were most highly correlated to components representing large-scale circulation. The biomass sustained by a given nutrient concentration in the Atlantic EBCs was twice as large as that of the Pacific EBCs. This apparent greater efficiency may be due to availability of iron, physical retention, or differences in planktonic community structure.
© 2003 Elsevier Ltd. All rights reserved.

1. Introduction

There has been an interest in defining the driving factors of the elevated biological production in the Eastern Boundary Currents (EBCs), i.e. the California, Humboldt, Canary, and Benguela Currents, since Ryther (1969) and Cushing (1969) explored global patterns of productivity. The high primary production in these regions is due to coastal upwelling and its variability impacts both the pathways of carbon and the local economies, as fisheries are large in the EBCs (FAO, 1999). The characteristic upwelling-favorable winds result from the quasi-stationary atmospheric high-pressure systems over the subtropical ocean basins. The upwelled water will have high nutrient concentrations if it originates below the pycnocline/nutricline. The equatorward-flowing EBCs are characterized by pycnoclines that shoal towards the coast, such that the top of the pycnocline is within the euphotic zone. Thus the large-scale wind and circulation patterns provide, respectively, the driving force for upwelling and the optimal nutrient concentration for significant

*Corresponding author. Tel.: +1-818-354-5097; fax: +1-818-393-6720.
E-mail address: mec@pacific.jpl.nasa.gov (M.-E. Carr).

0967-0645/$ - see front matter © 2003 Elsevier Ltd. All rights reserved.
doi:10.1016/j.dsr2.2003.07.015

biological production. Carr (2002) compared potential production, estimated from satellite measurements of ocean color, sea surface temperature (SST), and photosynthetically available radiation (PAR), and attempted to evaluate the relationship between production and other environmental variables. Potential productivity was high: the total for all four EBCs of almost 1 Gt C yr^{-1} was ~2% of a global marine production of 40 Gt C, although their collective area represents only 0.3% of the global ocean. Maximum annual production for the first 24 months of measurements from the Sea-Viewing Wide-Field-of view Sensor (SeaWiFS) was observed in the Benguela Current, followed by the Canary, Humboldt, and California Currents. The highest average primary production occurred in the Benguela and Humboldt Currents but the area of chlorophyll concentrations surpassing 1 mg Chl m^{-3} was much greater in the Canary Current than in the Humboldt Current. The linear relationship between environmental forcing (e.g., offshore Ekman transport, SST) and production was weak for the 2-yr mean examined. Latitude had the highest correlation with productivity patterns, in an inverse relationship. Unlike the results of Ware (1992), the mean offshore transport was only weakly correlated with annual production.

The present study of production necessarily relies on the observed chlorophyll concentration, because satellite-based productivity is a derived variable. The seasonal progression of phytoplankton biomass in the EBCs measured from SeaWiFS is driven to the first order by upwelling (Thomas et al., 2001). However, comparison of the annual and semi-annual harmonic fits to the time series of chlorophyll and Ekman transport for the first 3 years of SeaWiFS revealed that forcing and biological response are in phase in relatively few regions and that maximum amplitudes in Ekman transport do not always correspond to those in chlorophyll (Thomas et al., 2001). Thus we have not been able to distinguish the driving factors of biological variability using remote sensing data alone.

The present study has a dual goal: first, we quantify the seasonal evolution of source water characteristics using the unique hydrographic and nutrient climatology of Kearns and Carr (2003). By combining the climatological data with satellite-derived information, we can describe the seasonal and meridional patterns of phytoplankton biomass and primary production in the context of the environmental variability. Our second objective is to understand the controlling factors of the observed spatio-temporal patterns of biomass and primary production. We quantify the primary driving forces in the environmental variability, namely upwelling intensity as measured by local wind forcing, the thermal response to upwelling, and the source water characteristics (due to large-scale circulation). We then estimate the correlation between the driving terms and the observed biological patterns. A quantitative understanding of environmental variability and its impact on biomass and potential production is relevant to understand possible changes in these systems under different forcing conditions over interannual or longer time scales, such as El Niño, increased stratification, or decreased winds.

2. Data and methods

2.1. Data sets

To understand forcing associated with large-scale circulation patterns, we used a new hydrographic climatology presented in a companion paper (Kearns and Carr, 2003). Here we focused primarily on temperature, salinity, and the concentrations of phosphate and oxygen. PO_4 is considered representative for macronutrients because it was available at greatest data density and thus provided the least noisy estimates. We will address patterns of differential nutrient use in a future study. The primary data sources for the climatology are the National Oceanographic Data Center (NODC) World Ocean Database 1998, the California Oceanic Cooperative Fisheries Investigation (CalCOFI), and the South African Data Center for Oceanography (SADCO). In each EBC and for each season (January through March: JFM, April through June: AMJ, July through September: JAS, and October through December:

OND), the hydrographic and nutrient data were interpolated vertically to and horizontally along approximately neutral surfaces, corresponding to the potential density (σ_θ) surfaces 23.0–27.4σ_θ units (every 0.1), for a total of 45 vertical levels. We used a maximum horizontal grid spacing of 0.167°. The resulting seasonal climatologies are optimal for a comparative study of the upwelling regions. They provide the distribution of nutrients at high spatial resolution, estimated in a manner consistent with the natural pathways of advective mixing, i.e., along quasi-neutral surfaces. They are unique in their applicability to quantify hydrographic patterns and nutrient dynamics in the EBC regions.

We used 'climatological' satellite data corresponding to the first three calendar years of SeaWiFS (1998, 1999, 2000). The chlorophyll concentrations measured by SeaWiFS (Version 4 from the August 2002 reprocessing) were used with concurrent wind vectors (from the 2nd European Remote-sensing Satellite, ERS2), SST (from the Advanced Very High Resolution Radiometer, AVHRR, Pathfinder Project), and PAR (from the SeaWiFS Project). Seasonal means were compiled to address the seasonal cycle and to compare with the hydrographic data. Monthly average fields at 0.5° (wind vector) and ~9 km (SST, chlorophyll, and PAR) were used. The alongshore component of wind stress and the offshore Ekman transport (also referred to as wind forcing, in $m^3\ s^{-1}\ m^{-1}$, hereafter $m^2\ s^{-1}$) were estimated using bulk formulae (Gill, 1982). The ΔSST is obtained at each 9 km pixel by subtracting the 1°-average SST at the coast from the SST ~5° offshore at the same latitude. It is a measure of the temperature difference moving offshore. Positive values indicate colder water (due primarily from upwelling) at the coast. The chlorophyll and primary production were averaged at each pixel in approximately 1° bins adjacent to the coast.

We estimated primary production with the algorithm developed by Howard and Yoder (1997), with modifications as explained in Carr (2002). Existing algorithms that estimate primary production from ocean color vary by a factor of two (Campbell et al., 2002; Carr and Friedrichs, 2002). An ongoing comparison of primary production algorithms indicates that this variant of the Howard and Yoder model produces close to multi-model average values at high chlorophyll concentrations (Carr and Friedrichs, 2002).

The source-water characteristics were estimated by designating the densest water in the upper 50 m in the pixel adjacent to the coast as the upwelling σ_θ surface. The depth and characteristics (temperature, salinity, and concentration of oxygen and PO_4) of that surface 1° offshore at the same latitude were taken to be those of the source water. The vertical excursion of the upwelling σ_θ surface, ΔZ, was the difference from the depth of the upwelling surface 1° offshore and the depth at the coast. The definition of 'source water' was tested by varying both the assumed depth of the 'shallow' near-shore layer (30 and 70 m) and the distance offshore (0.5–2°) to designate 'upwelling surface' and 'origin', respectively. The resulting spatial and seasonal pattern of source water characteristics changed negligibly. The distance offshore (as when deriving ΔSST) was estimated using degrees of longitude (pixels) and thus varies with latitude. It was not converted to a horizontal distance because upwelling dynamics depend on the Rossby radius of deformation which is also latitude-dependent. The derived characteristics of the source water were smoothed with a five-point median filter.

The ETOPO5 bathymetry, at 5-min resolution, was used to estimate the width of the continental shelf. We define the inner shelf as areas with water depth at or less than 100 m and outer shelf as areas of water depth at or less than 500 m. The data are smoothed with a 10-point median filter.

We divided each EBC into 5–6 regions characterized by the maximum biomass attained and the seasonal range of biomass and the forcing variables (Table 1). These regions are the same as in Carr (2002) (hereafter EBC1), with two exceptions: the southern boundary for the southernmost region in the Benguela Current is 36°S instead of 38°S, and the southern boundary for Region 6 in the Canary Current is 6°N instead of 5°N. The numbering scheme is such that region numbers increase moving towards the equator. In EBC1, the data started in September of 1997 and went to August 1999. The satellite data in this study period are from January 1998 to December 2000. Another

Table 1
Regions of the EBCs

Atlantic EBC	Regions	Limits	Pacific EBC	Regions	Limits
California	1	40°–48°N	Canary	1	35°–45°N
	2	34°–40°N		2	33°–35°N
	3	32°–34°N		3	27°–33°N
	4	26°–32°N		4	20°–27°N
	5	24°–26°N		5	11°–20°N
				6	6°–11°N
Humboldt	1	40°–33°S	Benguela	1	36°–35°S
	2	33°–27°S		2	35°–33°S
	3	27°–18°S		3	33°–29°S
	4	18°–15°S		4	29°–24°S
	5	15°–5°S		5	24°–19°S
				6	19°–15°S

difference is that primary production was estimated with climatological PAR values in EBC1, while here we use concurrent PAR provided by the SeaWiFS Project.

2.2. Approach

We aim to discern the environmental factors that control the observed meridional and temporal patterns of biomass and primary production, which we call production regimes. Is the governing factor local wind forcing, PAR, or nutrient supply? We expect each region to be governed by a different regime, so we carried out the analysis within each region. A straight correlation analysis between the observed patterns of driving terms (such as wind or nutrients) and those of biomass or production was inconclusive because the different driver variables were not always statistically independent. Therefore, we used principal component analysis to obtain a more robust characterization of the environmental variability in each region of the EBCs.

We focused on the space–time series of five variables: PAR, offshore transport, ΔSST, ΔZ, and the concentration of oxygen of the source water. These chosen variables are relatively distinct. Although they are correlated to various degrees in specific regions, the relationship among them varies widely, except for ΔZ and oxygen concentration. Both of these variables indicate the large-scale signature of the upwelling process: ΔZ, the displacement of the thermocline, represents the physical expression, while oxygen concentration indicates nutrient levels. We used O_2 rather than PO_4 because the original data density for O_2 was much greater than for PO_4 and there is a strong correlation between the two. Although generally related, ΔZ and O_2 concentration do not covary in all regions because of variability in source water masses. The resulting principal components provide a statistically sound characterization of the dominant environmental factors in each region. If two or more variables have a similar seasonal and meridional progression in a given region, they are combined together in a principal component, thus precluding any concern over independence of forcing terms.

To characterize the production regimes, we carried out a correlation analysis between the space–time series of the principal components and those of biomass and primary production. We also considered the width of the continental shelf as a potential driving factor. The linear correlation coefficient was estimated between the space–time series of biomass, and primary production, and the spatial series of shelf width and the space–time series of the three principal components within each region. The prevailing forcing regime is assumed to be that for which the correlation coefficient is greatest, while its environmental interpretation is given by the component scores.

3. Results

3.1. Seasonal fields of wind forcing and biomass

The seasonal average chlorophyll and wind speed fields are shown for all four EBCs in Fig. 1. Upwelling-favorable winds, i.e. alongshore and equatorward, are accompanied by increased concentration of chlorophyll along the coast. There is a general poleward progression of upwelling-favorable winds in hemispheric spring and summer (Bakun and Nelson, 1991). Although dependent on the large-scale circulation pattern of ocean and atmosphere, upwelling itself is a mesoscale process and occurs in a narrow band adjacent to the coast. The width of this band is given by the Rossby radius of deformation, a function of water depth, stratification, and latitude, which is about 10–30 km (Allen, 1973). The 'productive' band of high phytoplankton biomass and fisheries can exceed 100 km offshore (Ware, 1992; Carr, 2002). Filaments and jets extend the effects of coastal upwelling further offshore by advecting nutrient-rich water tens to hundreds of kilometers into the open ocean (Lutjeharms et al., 1991; Strub et al., 1991). The satellite wind speeds in Fig. 1 are in good agreement with historical wind fields (Bakun and Nelson, 1991). Chlorophyll concentrations surpass 1 mg Chl m^{-3} within 50–150 km of the coast. Seasonal maxima are generally concurrent with maximum alongshore winds.

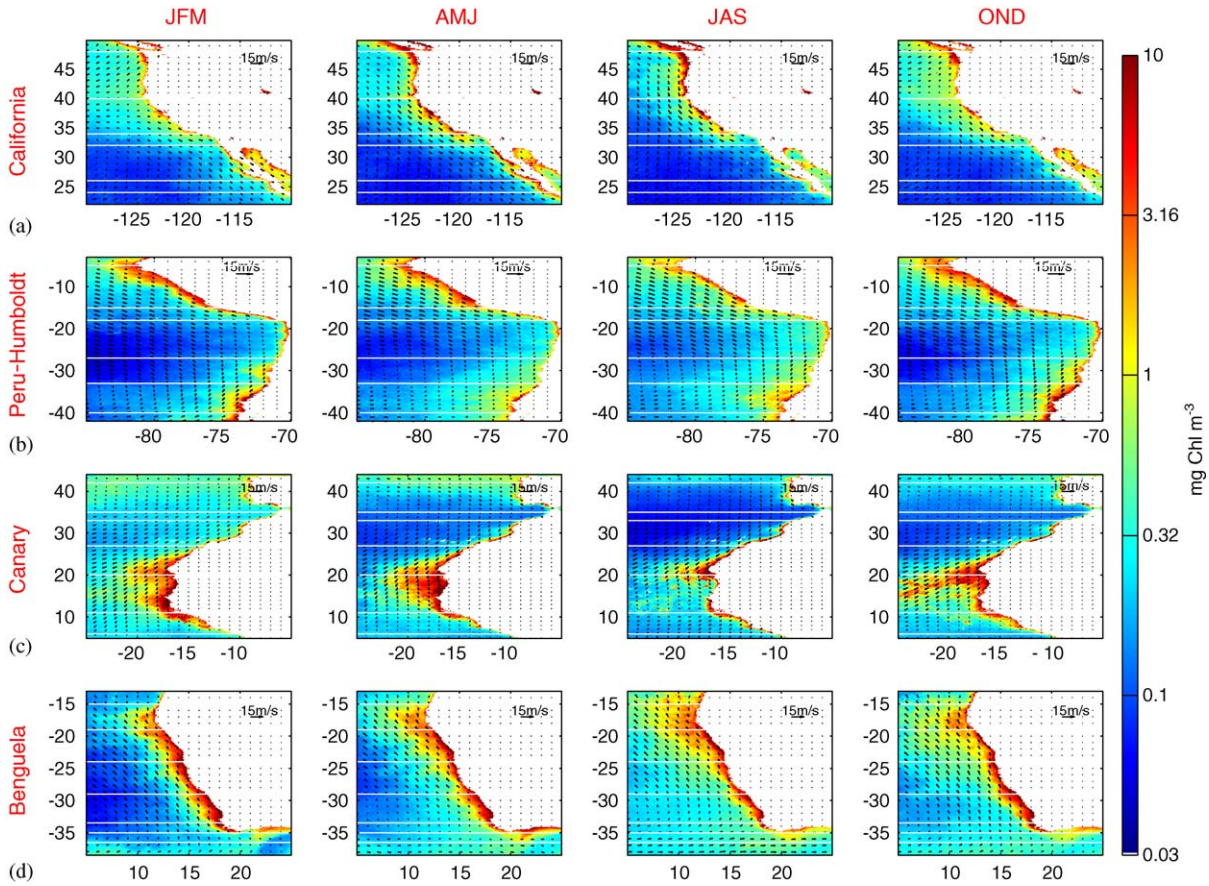

Fig. 1. Seasonal mean chlorophyll and wind vector for the period 1998–2000. (a) California, (b) Peru-Humboldt, (c) Canary, and (d) Benguela Currents. The regions from Table 1 are indicated by white horizontal lines.

The remaining analysis is based on coastal averages of the prevailing environmental variables, but Fig. 1 provides a broader context for the near-coastal processes analyzed later. Note for example the broad plumes of high chlorophyll that extend offshore from near 20°N in the Canary Current (Gabric et al., 1993), north of 20°S in the Benguela, and north of 10°S in the Peru-Humboldt. The averaging blurs the filaments that re-occur often in association with promontories or capes in regions subjected to high winds (> 10 m day^{-1}).

3.2. Seasonal and meridional variability of coastal properties

3.2.1. California Current (Fig. 2a)

The continental shelf in the California Current is very narrow: the outer shelf is ~50 km wide for most of the coastline between 32° and 48°N and becomes broadest between 32° and 28°N (even exceeding 150 km). The inner shelf extends 10 to 50 km offshore, except between 32° and 28°N where it can reach 100 km. The outer and inner shelf separate to form a gradual continental slope

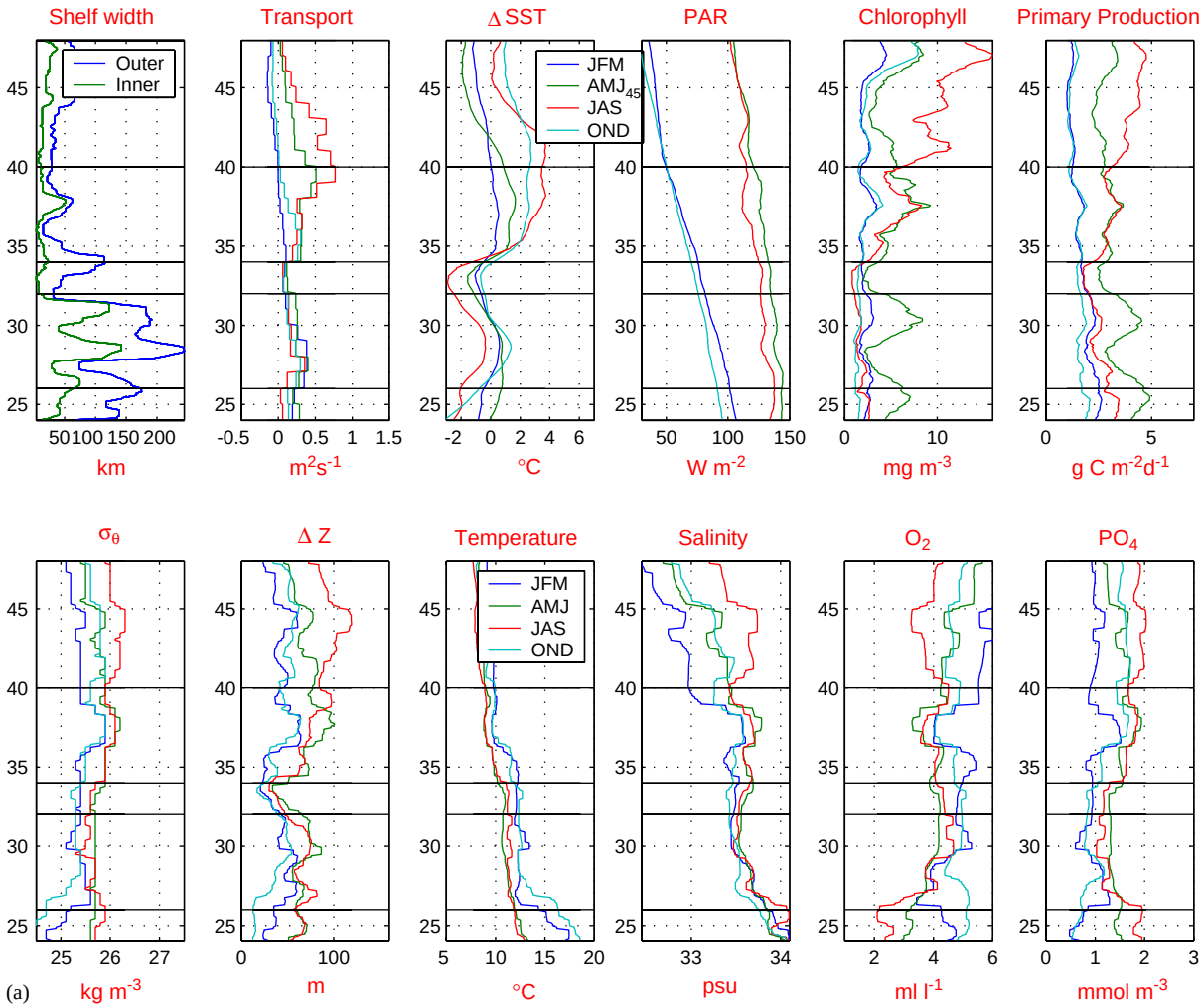

Fig. 2. Seasonal mean variables for the coastal band of the (a) California, (b) Peru-Humboldt, (c) Canary, and (d) Benguela Currents. The regions from Table 1 are indicate by black lines. JFM is in dark blue, AMJ in green, JAS in red, and OND in cyan.

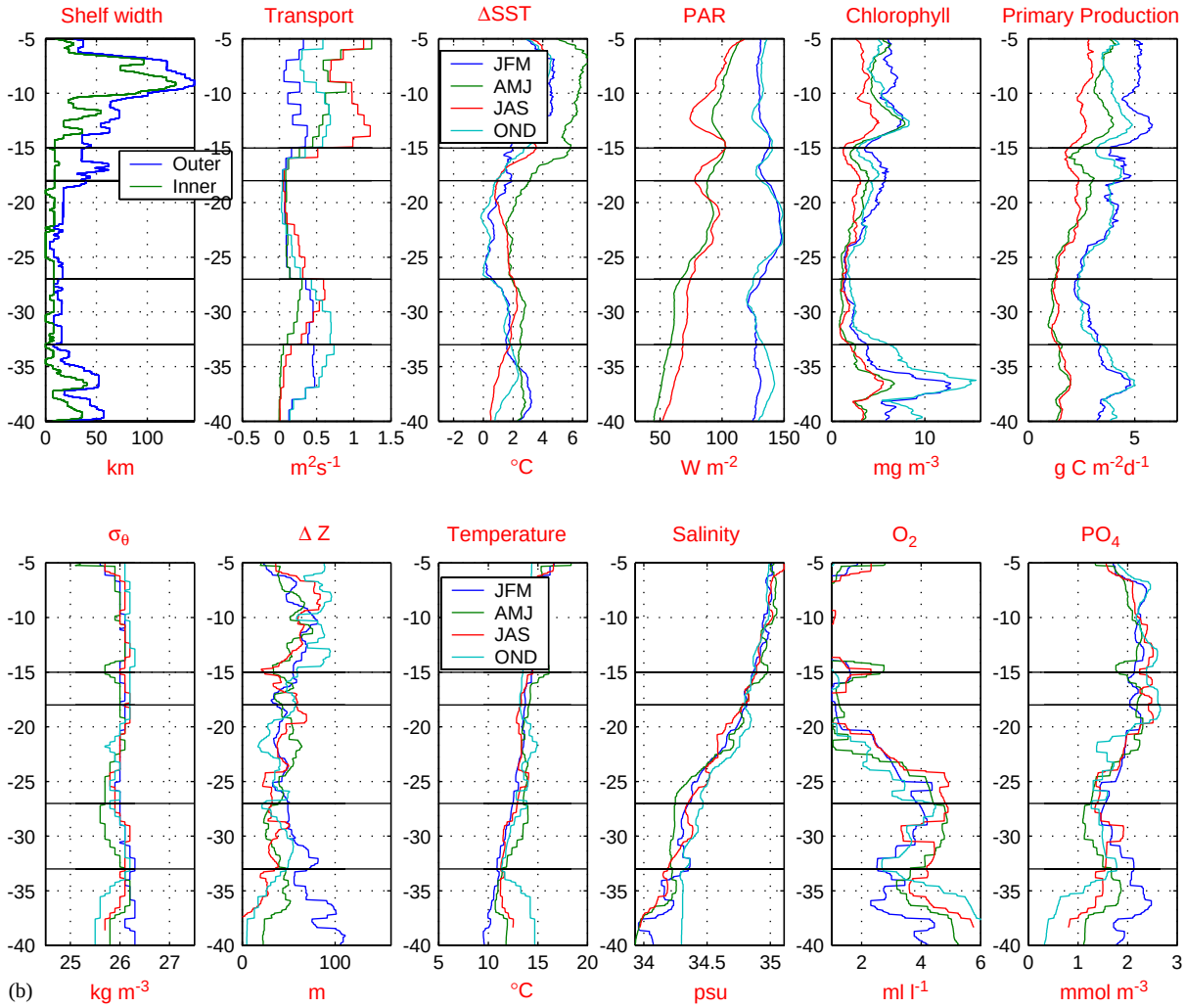

Fig. 2 (*continued*).

south of 32°N and near 34°N in the Southern California Bight (SCB).

Transports are typified by strong seasonal variability north of 34°N: the maximum is between 43° and 39°N (> 0.5 $m^2\ s^{-1}$) in JAS and it is negative in JFM and OND. South of 34°N, transport is less than 0.4 $m^2\ s^{-1}$ and although the seasonal progression varies, the strongest wind forcing is generally in AMJ. The SCB (32–34°N, Region 3) presents the weakest offshore forcing and minimal seasonal variability. The ΔSST generally parallels the wind forcing and presents peak values around 40°N (~4°C in JAS), an absolute minimum between 32° and 34°N (all seasons <0°C), and a secondary maximum at 27°N (OND). PAR is more than twice as large in AMJ–JAS than OND–JFM at 40°N (Region 1), but the difference lessens moving southward and minimum PAR values in OND are 100 W m^{-2} at 24°S. Chlorophyll concentration is maximum (3.2–10 mg Chl m^{-3}) in JAS north of 40°N (Region 1). South of 40°N the concentrations in AMJ track closely those of JAS until 34°N where AMJ becomes larger. Productivity surpasses

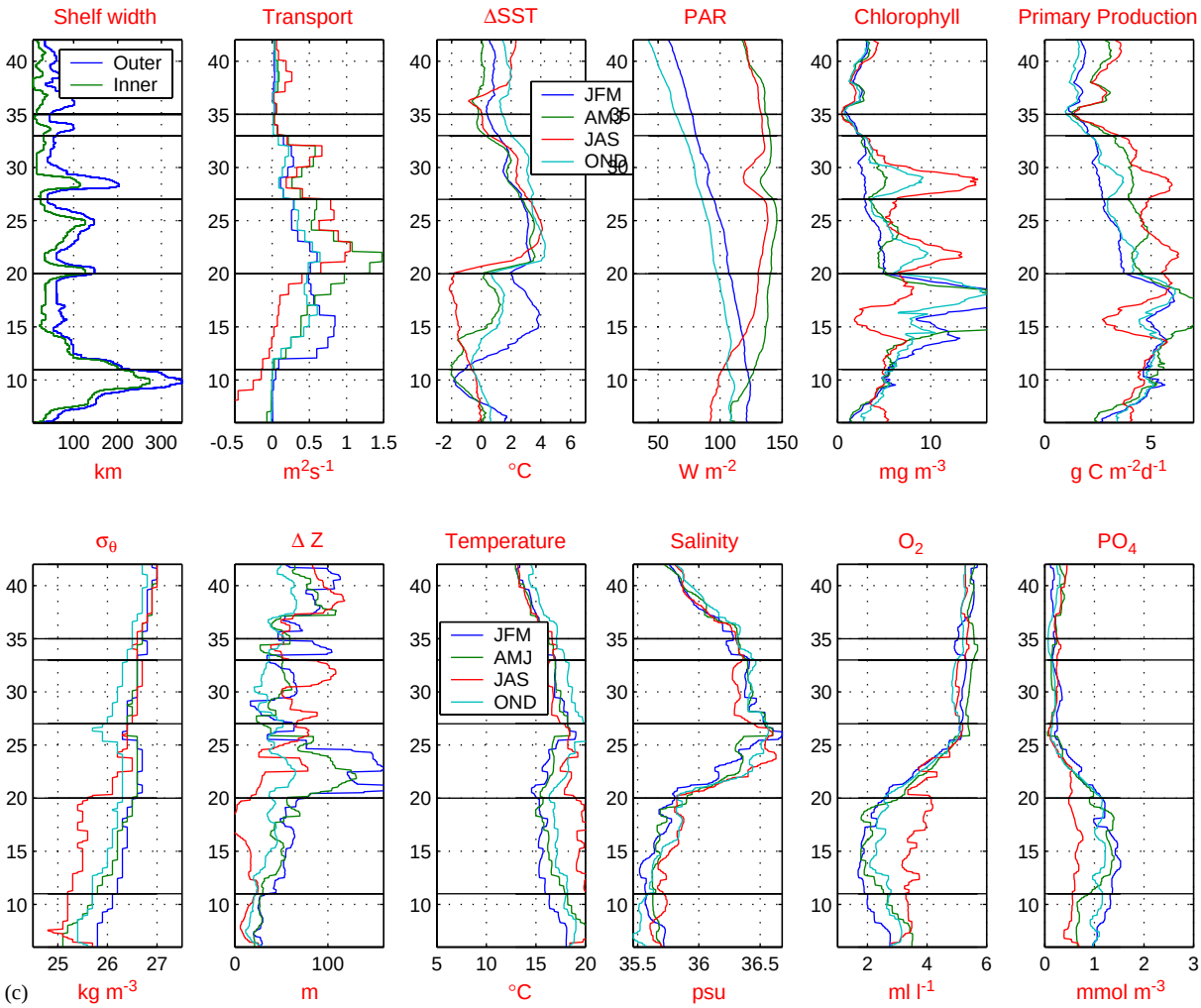

Fig. 2 (*continued*).

1.8 g C m^{-2} day^{-1} at all latitudes in JAS and AMJ, except for 32–34°N.

In the major upwelling season (AMJ–JAS) the upwelling density surface is 25.9 or greater north of 34°N, and between 25.5 and 25.7 to the south. The upwelling surface shoals 60 m or more in AMJ–JAS except in the SCB where ΔZ is ~40 m. Temperature/salinity of the source water increases/decreases to the south and the source water is coldest/most saline in AMJ–JAS. The oxygen concentration is minimum in JAS north of 36°N and in AMJ from 27 to 36°N. PO_4 concentrations of the source water are maximum (~2 mmol m^{-3}) in JAS north of 40°N and minimum in JFM (~1 mmol m^{-3}); south of 40°N, AMJ values track those in JAS to 35°N where they surpass them. This seasonal succession is also seen in chlorophyll concentration, ΔSST, and transport. The source water characteristics reflect the seasonal and spatial shifts in the subpolar versus subtropical origin for upwelling (Castro et al., 2001). Low-oxygen water from the Eastern Tropical North Pacific can penetrate as far north as 40°N in the undercurrent (Castro et al., 2001), while low-salinity waters from the subpolar gyre are advected southward to 30°N (Bernal and McGowan, 1981).

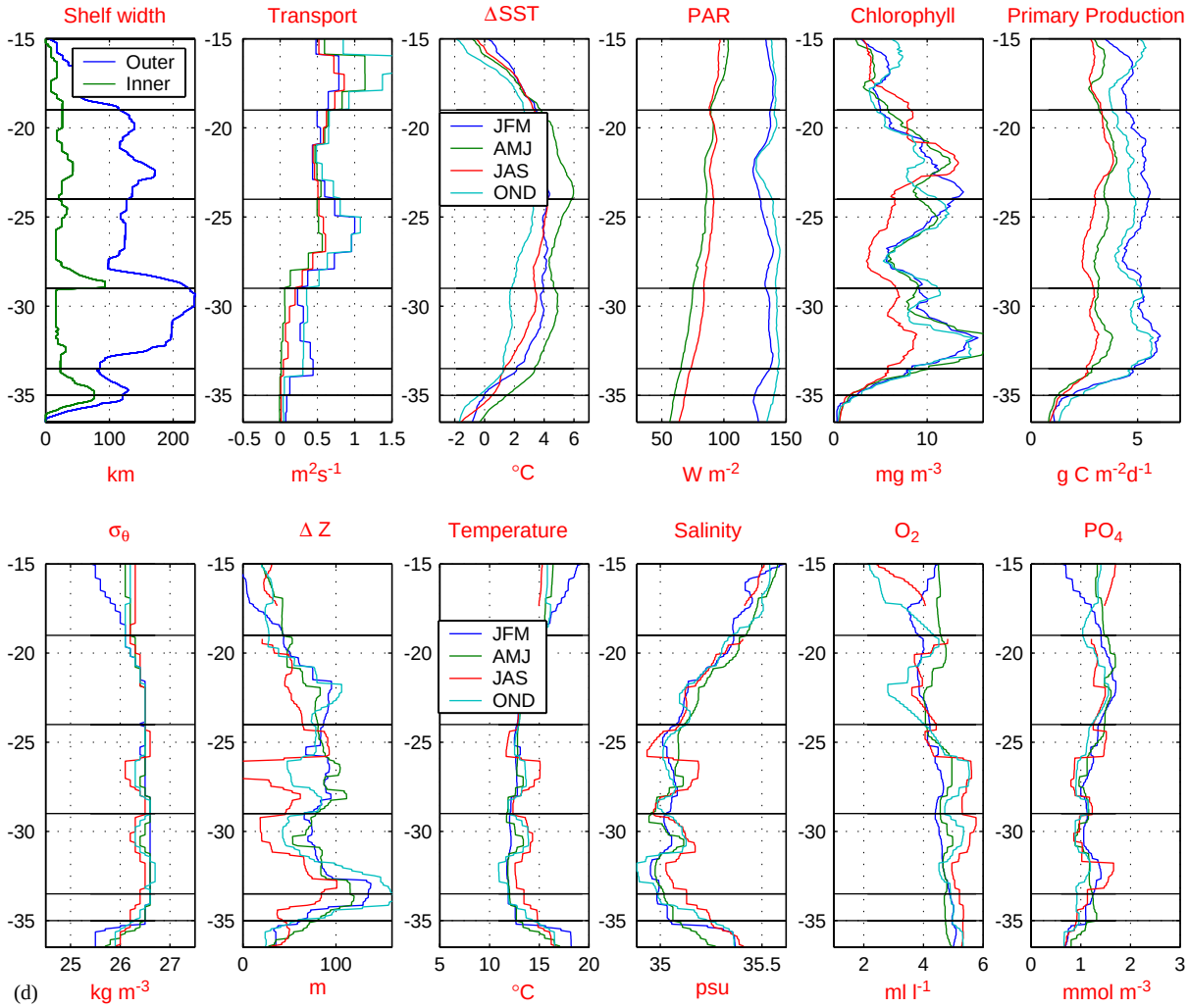

Fig. 2 (*continued*).

3.2.2. Peru-Humboldt Current (Fig. 2b)

The continental shelf is narrowest in this EBC, as both the inner and outer shelves are within 50 km between 15° and 35°S, and the continental slope is very steep, especially between 20°S and 34°S (Table 2). Between 7 and 10°S, both inner and outer shelves extend beyond 100 km.

Ekman transport is offshore year-round throughout this system. Maximum values (0.5–>1 $m^2\ s^{-1}$ in JAS) and peak seasonal range occur north of 15°S (Region 5) and between 22° and 40°S (Regions 1 and 2: > 0.5 $m^2\ s^{-1}$ in OND). Both transport and seasonal range are minimum between 16° and 22°S. Maximum ΔSST occurs in AMJ throughout most of the coast with maximum values (> 5°C) north of 15°S. PAR is maximum in OND and the seasonal range is a factor of ~2 south of 30°S. Biomass peaks in JFM north of 22°S and in OND to the south. The maximum exceeds 5 mg Chl m^{-3} north of 20°S and south of 35°S; seasonal range is maximum in these regions as well. Primary production has the same seasonal cycle as chlorophyll concentration and is maximum (> 4 g C m^{-2} day^{-1}) north of 18°S (JFM)

Table 2
Summary of prevailing conditions in different regions

		CS	LF						LS		BIO			
			W			ΔSST			PO_4		Chl		PP	
			Mx	Mn	T	Mx	Mn	T	Mx	T	Mx	T	Mx	T
Cal	1	50	0.4	0.1	JAS	2	0.4	OND	1.9	JAS	11	JAS	4	JAS
	2	40	0.4	0.2	JAS	3	1.6	JAS	1.3	JAS	6	AMJ	3	AMJ
	3	60	0.1	0.08	AMJ	0	−1	OND	1.3	AMJ	3	AMJ	4	AMJ
	4	155	0.3	0.2	AMJ	0.4	0	OND	1.7	AMJ	5	AMJ	4	AMJ
	5	140	0.2	0.15	AMJ	0.4	−1	AMJ	1.9	JAS	6	AMJ	5	AMJ
Per	1	40	0.4	0.2	OND	2.6	2	JFM	1.4	JFM	9	OND	4	OND
	2	13	0.6	0.4	OND	2.5	2	AMJ	1.5	JFM	3	OND	3	JFM
	3	15	0.2	0.1	JAS	2	1	AMJ	1.8	JFM	3	OND	3	OND
	4	40	0.2	0.2	JAS	4	2	AMJ	2.3	OND	5	JFM	4	JFM
	5	80	0.9	0.6	JAS	6	4	AMJ	2.1	OND	6	JFM	5	JFM
Can	1	60	0.1	0.06	JAS	1.7	0.9	OND	0.3	JAS	2	JFM	3	JAS
	2	70	0.06	0.04	JAS	1.7	0.6	OND	0.3	JAS	1.7	JFM	2	JAS
	3	80	0.4	0.3	AMJ	3	0.6	2	0.3	OND	7	JAS	5	JAS
	4	100	0.9	0.6	AMJ	3.6	3	2	0.6	JFM	8	JAS	5	JAS
	5	90	0.6	0.4	JFM	2.4	0.3	JFM	1.3	JFM	11	AMJ	6	AMJ
	6	190	0	−0.1	JFM	0	0.2	OND	1.2	JFM	5	JAS	4	OND
Ben	1	60	0.08	0.03	JFM	0.5	−0.4	AMJ	0.9	AMJ	1	OND	2	OND
	2	100	0.2	0.1	JFM	2.6	1.3	AMJ	1.3	AMJ	5	OND	4	OND
	3	180	0.2	0.2	OND	4.4	3	AMJ	1.2	JFM	12	AMJ	5	JFM
	4	130	0.8	0.6	OND	4.8	4	AMJ	1.2	AMJ	9	OND	5	JFM
	5	140	0.6	0.5	OND	5	4	AMJ	1.6	AMJ	9	JAS	5	JFM
	6	50	1.2	0.9	OND	2	1.5	JFM	1.6	JAS	5	OND	4.5	JFM

CS refers to the outer shelf width in km, LF includes wind forcing (W in $m^2\ s^{-1}$) and ΔSST (in °C), LS refers to PO_4 concentration (P in mmol m^{-3}), and BIO refers to chlorophyll (Chl in mg Chl m^{-3}) and primary production (PP in g C m^{-2} day^{-1}). Mx is the maximum seasonal mean and Mn is the annual average, T is the season at which the maximum value is observed.

and south of 34°S (OND) and minimum at 27°S (~2 g C m^{-2} day^{-1})

Water for upwelling comes from σ_θ surfaces between 25.6 and 26.2. The vertical displacement of the upwelling surface (ΔZ) is less than 50 m between 15 and 34°S. The water mass characteristics confirm that source water is primarily equatorial subsurface water (ESSW) north of 18°S and subAntarctic water (SAW) south of that; beyond 35°S there is an influence of Antarctic intermediate water (AIW) (Blanco et al., 2001). The two water masses are clearly distinct in terms of salinity (ESSW between 34.8 and 35; SAW ~ 34.3) and oxygen concentration (ESSW < 2 ml l^{-1}, SAW ~ 4 ml l^{-1}). The salinity of the source water does not vary seasonally north of 18°S, while to the south meridional excursions of the front between ESSW and SAW appear as salinity variability. The PO_4 content of the source water is the highest of all EBCs and exceeds 2 mmol m^{-3} north of 20°S (in ESSW) and south of 34°S (perhaps an AIW influence). The seasonal variation in source water characteristics reflects the poleward transport of ESSW in the undercurrent (maximum in AMJ, spring) and the equatorward transport of SAW (maximum in JAS, winter) as seen in salinity and oxygen. The minima in nutrient concentration of the source water near 27°S are reflected in the chlorophyll concentrations. Friedrich and Codispoti (1981) located the

front between SAW and ESSW at 15°S and found maximum influence of low nutrient-high O_2 SAW in JAS (which is also the strongest upwelling period). The influence of SAW is greatest also in JAS in this study but maximum variability is observed at 18°S rather than 15°S. Friedrich and Codispoti (1981) used a single fixed density surface ($\sigma_\theta = 26.0$), while in this study the upwelling density surface is different at each location and season. We believe that a seasonal shift in upwelling density surface may be more realistic.

3.2.3. Canary Current (Fig. 2c)

The width of the outer shelf is generally 100 km north of 12°N but it broadens to 300 km at 10° and then decreases again. The separation between inner and outer shelf is fairly consistently ~50 km, indicative of a uniform slope.

Ekman transport is largest between 11° and 27°N (Regions 4 and 5). The seasonal maximum is in JFM between 12° and 16°N, in AMJ from 16° to 22°N (the EBC absolute maximum, $> 1.5\ m^2\ s^{-1}$), and in JAS north of 22°N. South of 11°N (Region 6) and north of 27°N (Regions 1–3) transport is at most $0.5\ m^2\ s^{-1}$ and varies little seasonally. The meridional and seasonal variation of ΔSST is similar, except that it peaks in OND from 27° to 37°N. The EBC maximum ΔSST exceeds 3°C between 20° and 34°N (primarily in OND). PAR varies by over a factor of two north of 30°N, while to the south of 10°N PAR is less in JAS–AMJ than in OND–JFM. Phytoplankton concentrations north of 30°N are less than 3.2 mg Chl m^{-3} and present negligible meridional or seasonal variation. Local maxima occur in JAS and OND at 28°N and between 15° and 20°N in AMJ and JFM (> 10 mg Chl m^{-3}). Maximum seasonality is observed between 11 and 20°N (Region 4), where the front in SST travels seasonally (not shown). Peak primary production occurs in JAS from 42° to 20°N (Regions 1–4) and generally in AMJ to the south. Productivity increases southward from ~2 g C m^{-2} day^{-1} at 33°N to ~5.6 g C m^{-2} day^{-1} at 20°N where it remains uniform to 9°N.

Source water for upwelling comes from σ_θ surfaces heavier than 26.0 north of 11°N and lighter to the south. ΔZ exceeds 100 m between 20° and 25°N in JFM. It is generally 50–100 m at some season north of 25°N and below 50 m south of 20°N. Temperature of the source water increases from 40° to 25°N and is minimum between 25°N and 10°N in all seasons except JAS. Salinity is maximum (~36.25) between 33° and 22°N, and falls to minimum values (~35.7) south of 20°N. Seasonal variability of temperature, salinity, and nutrients between 10° and 26°N reflects the frontal region between South Atlantic Central Water (SACW) and North Atlantic Central Water (NACW) near 20°N (Codispoti and Friedrich, 1978; Fraga et al., 1985). In the present study maximum penetration of SACW occurs in JFM, while salinity and temperature are maximum in JAS, consistent with maximum southward transport of NACW. The oxygen concentration is order $5\ ml\ l^{-1}$ to 25° and $<2\ ml\ l^{-1}$ between 10° and 19°N. Nutrient concentrations reflect the distinction between SACW (> 1 mmol m^{-3}, south of 20°N) and NACW with $PO_4 < 0.5$ mmol m^{-3} north of 25°N.

3.2.4. Benguela Current (Fig. 2d)

This region has the smoothest sloping shelf: ~100 km separate the inner and outer shelves. The inner shelf width is similar to that of the other EBCs but the outer shelf surpasses 100 km south of 19°S and extends beyond 200 km between 28° and 32°S.

Maximum offshore Ekman transport approaches or exceeds $1\ m^2\ s^{-1}$ in OND north of 19°S (Region 6) and between 24 and 29°S (Region 4). Transport consistently surpasses $0.5\ m^2\ s^{-1}$ north of 28°S while that is the maximum value to the south. Peak transport occurs generally in OND and JFM. ΔSST is maximum at 25°S (~6°C) and surpasses 4°C from 20° to 32°S (AMJ); it decreases to the north and south, changing sign at 16° and 35°S in almost all seasons. Chlorophyll concentration is almost uniform with latitude, with values exceeding ~5 mg Chl m^{-3} between 18° and 33°S. Local minima occur at 17° and 26°S (coinciding with local maxima in transport) and 30°S. The maximum is at 33°S (> 15 mg Chl m^{-3} in JFM), and values near 10 mg Chl m^{-3} occur at 28°S (OND) and between 25° and 21°S (JAS and AMJ).

Seasonal variation is weak with JAS (winter) maxima north of 22°S and JAS minima south of that. Productivity is even more uniform with latitude (5–6 g C m^{-2} day^{-1} in OND–JFM) with minima at 26°S and south of 35°S.

Source water for upwelling comes almost uniformly from the $26.5\sigma_\theta$ surface between 20° and 35°S. ΔZ exceeds 50 m between 20, and 35°S, and 100 m between 22° and 30°S and near 34° in JFM or OND. The temperature and salinity of the source water generally vary little seasonally. Maximum values are observed north of 20° and south of 34°S. The characteristics of the source water are consistent with the water mass described as 'upwelled Benguela Current Water': 12–18°C, 34.9–35.2 psu, with Angolan water in the northern extreme (17–22°C, 35.5–35.9 psu) and oceanic water, perhaps of Agulhas origin, to the south (16–20°C, 35.2–35.5) (O'Toole, 1980). Oxygen concentration increases from 3–4 ml l^{-1} north of 25°S to > 5 ml l^{-1} south of 35°S. PO_4 concentrations are maximum (> 1.5 mmol m^{-3}) between 19° and 24° (Region 5) and minimum (0.8–1 mmol m^{-3}) from 25 to 32°S (Regions 3 and 4) in JAS and OND coinciding with the salinity and temperature minimum. The observed nutrient levels are consistent with a SACW source water, with PO_4 ranging between 0.9 and 1.6 mmol m^{-3} (Bailey, 1985). The source water characteristics are in general good agreement with those presented by Jones (1971) for the southern Benguela, but they are more saline, warmer, and lower nutrient than those described by Calvert and Price (1971) for the northern Benguela, or Andrews and Hutchings (1980) for the southern. It is possible that differences in the identification of the upwelling surface may explain these discrepancies.

3.2.5. Regional summary

As discussed above (Fig. 2) and seen in the summary of the regional means in Table 2, the maxima in wind forcing, ΔSST, PO_4 concentration, and biological response are rarely concurrent. A temporal delay between wind forcing and the oceanographic and biological response is consistent with the paradigm. However in some regions (e.g. Regions 4 and 5 of the Peru-Humboldt Current, or Region 1 of the Canary), the biomass peak is out of phase with the maximum in transport or ΔSST.

In the Benguela and Canary Currents (Table 2), maximum biomass (> 6 mg Chl m^{-3}) is observed where the continental shelf is widest (> 80 km). There is at least one region in each current where peak transport surpasses 0.4 m^2 s^{-1}; these regions present peak chlorophyll concentrations in excess of 6 mg Chl m^{-3}. Both transport and ΔSST are generally weakest in the California Current despite comparable biomass and productivity to the other EBCs. Similarly, nutrient concentrations are lower in the Atlantic EBCs (at most 1.6 mmol m^{-3}) even though the biomass is no less than in the Pacifice EBCs, in which peak PO_4 surpasses 1.3 mmol m^{-3} in all regions.

The discrepancy between chlorophyll and production is most marked in seasonality. Maximum primary production occurs in hemispheric spring or summer because of maximum PAR. The exception is the winter maximum at 6–11°N in the Canary Current (which in fact coincides with peak PAR). Maximum biomass occurs always in summer or spring in Pacific EBCs and generally also in the Atlantic EBCs. Biomass is maximum in winter in the northern Benguela (Region 6 and the northern part of Region 5) and in the southern part of Region 5 in the Canary Current (coinciding with peak transport); in both cases at low latitudes (~12°N and <20°S). Fall maxima of biomass occur in the northern regions of the Canary Current. High biomass values in the Benguela Current are seen in all seasons, with minimal seasonal range.

3.3. Quantitative estimate of environmental variability

An obvious difficulty in our goal to characterize the primary driving forces within our study regions is that the environmental variables are correlated, and more frustratingly, to varying degrees in each region. In the general paradigm of coastal upwelling, large-scale upwelling implies a shoaling thermocline and cold water nearshore (positive ΔSST and ΔZ). When large-scale circulation is in concert with local wind forcing, Ekman transport and ΔSST should be positively correlated. Since

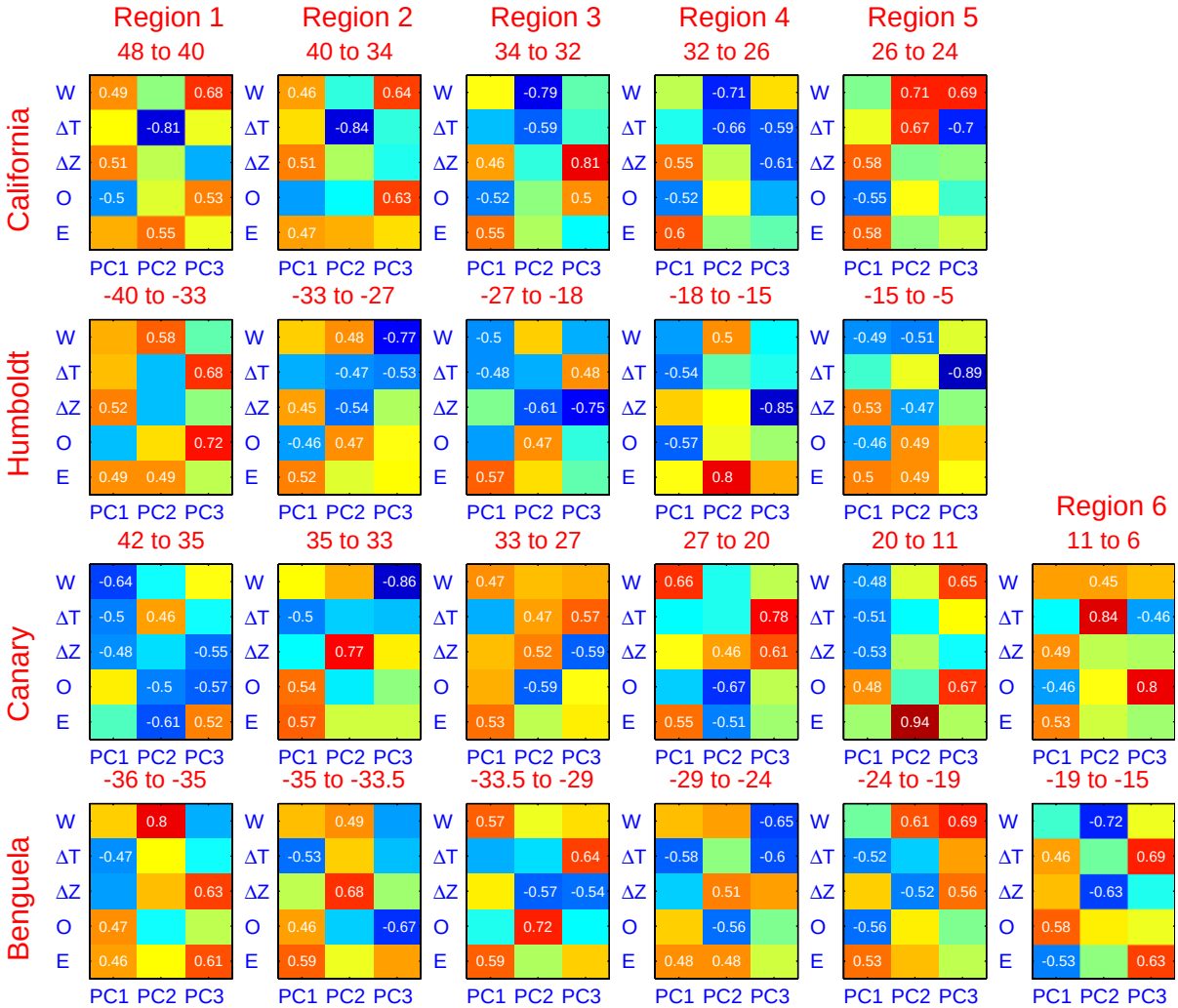

Fig. 3. Weights assigned to the variables for the first three components obtained from the principal component analysis of each region. Weights exceeding an absolute value of 0.45 are given in white.

oxygen concentration is inversely proportional to nutrient concentration, we expect the ascribed weight to have the opposite sign to those of ΔZ, ΔSST, and offshore transport. PAR is determined to the first order by latitude and to second order by cloud cover. Each region presented a somewhat different relationship between the driving terms within the general upwelling process. It was necessary to statistically group the variables that were correlated within each region.

We carried out principal component analysis with five variables (offshore transport, ΔSST, PAR, ΔZ, and O_2 concentration) to obtain an objective description of the observed variability within each region. The first two components (PC1 and PC2) explained 64% to 96% of the observed variability and the first three (PC1, PC2, and PC3) accounted for 86% to 99%.

To interpret the environmental meaning of the components, we examined the distribution of weights (Fig. 3). It is common that two or three variables present comparable weight in absolute value (where 'comparable' is defined as a difference of less than 0.1 between the two largest

Table 3
Environmental interpretation of each principal component

		1	2	3	4	5	6
Cal	PC1	LS/LF	LS/LF	E/LS	E/LS	E/LS	
	PC2	−T	−T	−LF	−LF	LF	
	PC3	LF/ − LS	LF/ − LS	LS	−T	−T	
Per	PC1	LS	E/LS	E/ − LF	LS/ − LF	LS/E/ − LF	
	PC2	LF	−LS	−LS	E/LF	−LF/ − LS	
	PC3	−T	−LF	−T	−T	−T	
Can	PC1	−LF/ − LS	E/ − LS	E/LF	LF	−LS/ − LF	E/LS
	PC2	−E	LS	LS	LS	E	LF
	PC3	−LS	−LF	−T	LS	LF/ − LS	−LS
Ben	PC1	−LS	E/ − LS	E/LF	−LS/E	LS/E	−LS/ − E
	PC2	LF	LS/LF	−LS	LS/E	LF/ − LS	−LF
	PC3	−T/E	LS	−T	−LF	LF	−T/E

LS denotes large-scale circulation, LF local forcing, E is PAR, T refers to negative gradient. The sign denotes the sign of the weight of the variables and they are listed in order of weight (Fig. 3).

weights and less than 0.12 between the highest weight and the third highest in a given component). This is especially clear for the first principal component (PC1), which explains the bulk of the variance. We used the weights, and their signs, to ascribe an environmental meaning to the components (Fig. 3 and Tables 3 and 4).

Two broad categories stand out: environments in which the spatial and temporal patterns were most strongly weighted by local forcing and those weighted by large-scale circulation. Two additional categories reflect PAR and an inverse function of the temperature gradient. A hybrid category arose when variables referring to both large-scale and local forcing have similar weights (with either the same or opposite sign).

- *Local forcing* is indicated by offshore transport, or ΔSST when the weights have the same sign. Eleven components were interpreted to represent local forcing, only one of which was PC1 and seven were PC2. Components driven by local forcing explained 12% to 37% of the observed variance.
- *Large-scale circulation* is indicated by oxygen concentration and/or ΔZ. In some regions, oxygen concentration is not a good proxy for large-scale circulation because of the low-nutrient content of the source water mass (e.g. NACW in Region 1 the Canary Current). Thirteen components were characterized by large-scale circulation; unlike local forcing, almost half of them were PC1. They explained between 8% and 83% of the observed variance.
- *Large-scale and local*: In the components for 12 regions, the weights were high for both large-scale circulation and offshore transport (though the sign is reversed in half of them, Tables 4a and 4b). These components explained between 7% and 69% of the observed variability. Although transport had the largest weight in six of these regions, only one of the six was PC1. When large-scale and local forcing explained most of the observed variance (PC1), they usually had the same sign and the large-scale weighed more than local forcing (Table 4b). Conversely, the impact of the component is generally less (PC2 or PC3) when the two forcing mechanisms have different signs or when local forcing is more important (Table 4b).
- *PAR* had the largest weight for PC1 in almost half of the regions (10). In seven of the 10 ten

Table 4
Table 4a shows the number of regions assigned to each category of environmental meaning. Table 4b shows the importance of other variables in regions assigned the hybrid category of LSLF and the PAR category

Variable	PC1	PC2	PC3
(a)			
LF	1	7	4
LS	5	7	1
LSLF	6	3	3
T	0	2	10
E	10	3	0
(b)			
LS/LF	5	1	0
LF/LS	1	2	3
Same	4	2	0
Not same	2	1	3
E	0	2	0
E/LS	7	0	0
E/LF	3	1	0

The order of variables in Table 4b is in order of decreasing weight; Same denotes that the large-scale variables and local forcing present consistent signs while Not same denotes that they have opposite signs. In the PAR category we distinguish between PAR alone, PAR with large scale (E/LS) and PAR with local forcing (E/LF) regardless of the relative sign of the weights.

regions, the weight for large-scale forcing was also significant, while in four, local forcing was co-dominant. PAR was also the single highest-weighted variable for PC2 in three regions. The components that were primarily driven by PAR explained 21% to 65% of observed variability. However, since PAR was accompanied by large-scale or local forcing in 77% of cases where it had a dominant weight, we consider this a secondary category.

- *Negative gradient* represents offshore gradients which are counter to those expected for upwelling (warmer inshore water). ΔSST represents both the large-scale circulation and real-time local forcing. There are three possible interpretations for a component weighted heavily by ΔSST. When the weight for ΔSST and transport is of the same sign, the component was ascribed to local forcing. When the weight for ΔSST is of the same sign as ΔZ (or inverse of oxygen) the component was categorized as large-scale circulation. But in 12 components (two in PC2 and 10 in PC3), the largest weight of the component is ascribed to ΔSST and the sign opposes that expected for either large scale or local forcing. In these cases the component was categorized as negative gradient. In about half of them, ΔZ (instead of ΔSST) presented a weight comparable, but of inverse sign, to that expected given the weight of oxygen, ΔSST, or transport. Components characterized by negative gradient explain at most 22% of variance (on average 14%) and are usually PC3.

3.3.1. Physical interpretation of components for each EBC

Fig. 4 and Tables 3 and 4 summarize the physical interpretation of the components for each region. PC1 was dominated by the large-scale circulation alone or coupled to local forcing and PAR. This is especially clear for the Pacific EBCs. In the Atlantic EBCs local forcing rose to prominence in PC1. PC2 was generally driven by local forcing, alone or coupled to large-scale circulation or to PAR (Table 4a). PC3 was primarily driven by negative gradient and local forcing (alone or in association with large-scale circulation).

In the California Current PC1 accounted for 54% to 71% of the variance. In all regions, PC1 represented large-scale circulation, coupled to local forcing or PAR, while PC2 (18–37% of variance) and PC3 (7–13% of variance) were associated with either local forcing (alone or in reverse sign to large-scale circulation) or with negative gradient.

In the Peru-Humboldt Current PC1 explained 42–65% of the observed variability. As in the case of PC1 in the California Current, large-scale circulation dominated, coupled to local forcing and PAR; an exception was Region 3 where PAR and local forcing had the largest weights. PC2 (18–38% variance explained) and PC3 (11–22% of variance) represented primarily local forcing (alone, with PAR, or with large scale) and negative gradient.

The first three principal components in the Canary Current accounted for 37–64%, 20–37%, and 8–17% of the variance. PC1 was weighted

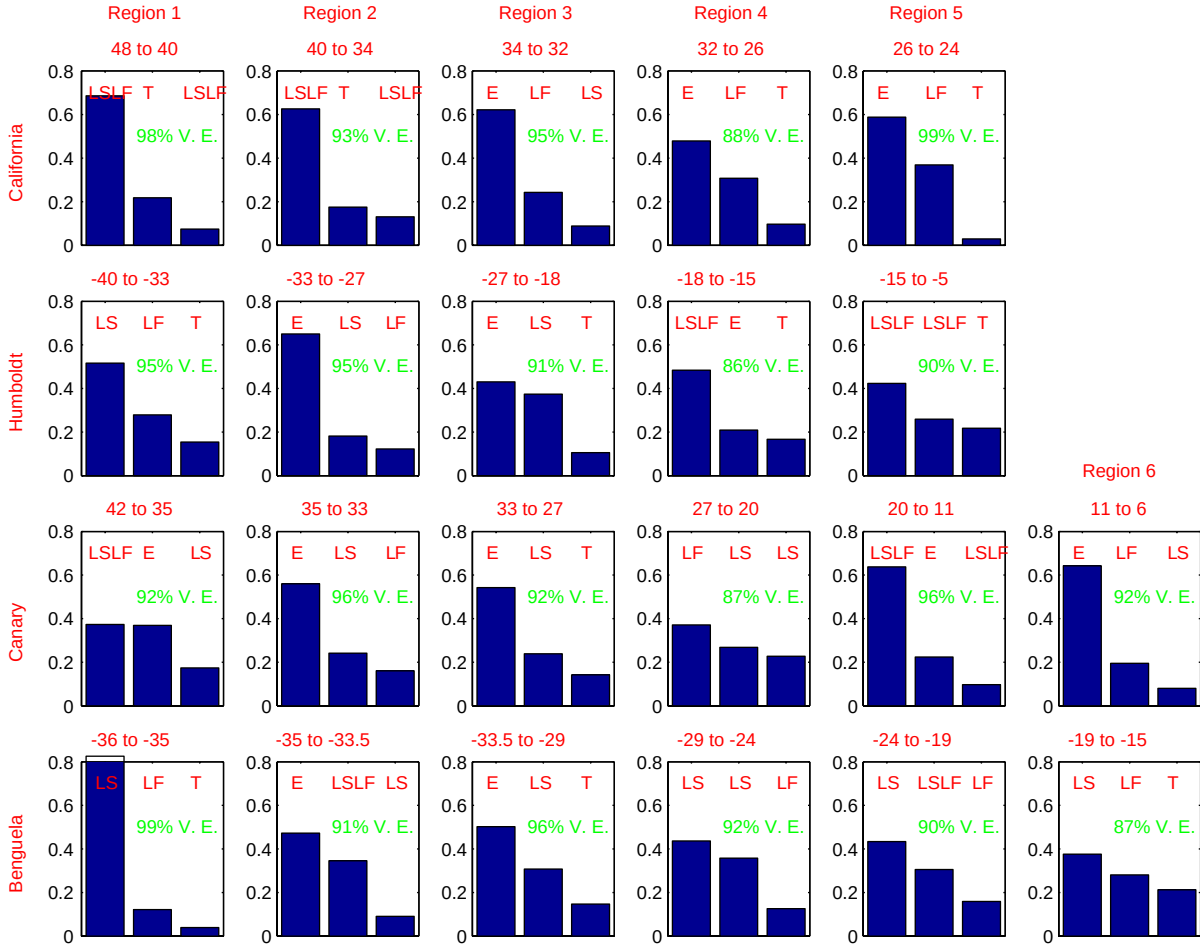

Fig. 4. Variance explained by each component and summary of the environmental meaning. See Table 4 for more details and nomenclature.

heaviest by PAR with largest scale or with local forcing and in two regions both local and large scale were important. PC2 and PC3 were generally large-scale dominated.

In the Benguela Current PC1 accounted for 32–82% of the observed variability and primarily represented large-scale patterns and PAR. PC2 explained 12–36% of the variance and was determined by local forcing, alone or in combination with large scale. In two regions large scale was dominant. PC3, explaining 4–21% of variance, was negative gradient in half the regions and local forcing in two.

3.4. Production regimes

Having characterized the environmental forcing of each region with the principal components, we used them to quantify the production regimes. In addition to the principal components, we also evaluated the impact of the width of the continental shelf. We calculated the linear correlation coefficient between the time–space series of biomass and primary production and the driving factors (spatial series of shelf width and the space–time series of the three principal components). The prevailing forcing regime was assumed to be that

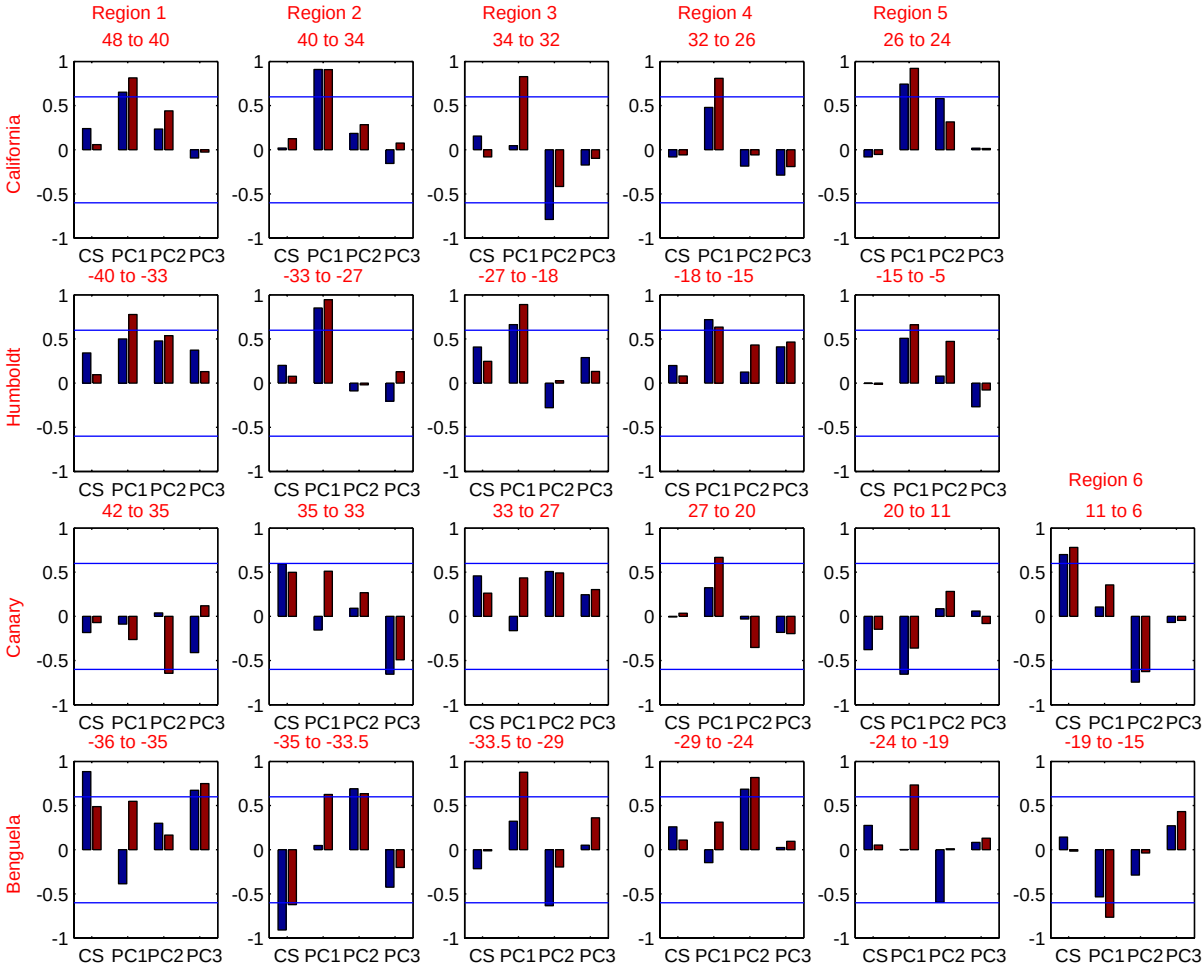

Fig. 5. Correlation coefficient between the driving factors (i.e. the continental shelf CS, and the first three principal components -PC1, PC2, PC3) and chlorophyll (blue) and primary production (red). The horizontal blue lines indicate $r = \pm 0.6$. The time–space series are such that the degrees of freedom surpass 100 in almost all regions and the correlation coefficients are significant to $p < 0.001$.

for which the correlation coefficient was greatest. Fig. 5 shows the correlation coefficient of biomass (blue) and primary production (red) with each of the four driving factors. The horizontal lines in Fig. 5 denote ± 0.6. Given the length of the time–space series, only five regions have fewer than 100 degrees of freedom and the significance level of the correlation coefficient is at $p < 0.001$ in all cases.

In most regions there was a clearly preferred component for chlorophyll and primary production (Fig. 5). Also, for 68% of the regions, both biological variables were most highly correlated to the same factor. In five of the seven cases in which the primary driving factor for chlorophyll was different from that for primary production, primary production was determined by a component driven by PAR.

The primary driving factor for biomass was most frequently large-scale forcing, alone and together with local forcing, while the primary driver for primary production was most frequently PAR and the hybrid regime of large scale and local forcing (Table 5, Fig. 6). Local forcing alone was correlated to biomass (primary production) in

Table 5
(a) The assignment of primary driving force for the time–space series of chlorophyll concentration and primary production in each region. When the primary driving force for primary production is different from that of biomass it is given in parenthesis. (b) The summary of the number of regions assigned to each category. (c) More details about the relative order and sign of the variables; the nomenclature is the same as in Table 4b

(a)

	1	2	3	4	5	6
California	LS/LF	LS/LF	LF (E/LS)	E/LS	E/LS	
Peru	LS	E/LS	E/ − LF	LS/ − LF	LS/E/ − LF	
Canary	LS (E)	LF (E/ − LS)	LS	LF	LS/LF	−LF (CS)
Benguela	CS (T)	LS/LF	LS (E/LF)	LS	−LF/LS (LS)	LS/E

(b)

Variable	CHL	PP
LSLF	7	6
E	4	8
LS	6	5
LF	4	1
T	0	1
CS	1	1

(c)

Variable	CHL	PP
LS/LF	4	4
LS/ − LF	3	2
LF	3	1
−LF	1	0
E/LS	3	4
E/ − LS	0	1
E/LF	0	1
E/ − LF	1	1
E	0	1

only four (one) regions. Local forcing was negatively correlated with chlorophyll concentration in Region 6 of the Canary and Region 5 of the Benguela. The correlation was positive to a negative weighting of local forcing in Regions 3–5 in the Peru-Humboldt Current. These negative correlations to local forcing (or positive correlation with components which have negative weights on local forcing) indicate an advective effect in which biomass is lost from the region for increasing transport rates. Large-scale circulation had a negative correlation in only one case (primary production in Region 2 of the Canary Current). PC1 in this case was highly weighted by PAR and oxygen concentration (positive). The source water in this region is NACW, the nutrient supply is minimal, and the change in oxygen concentration almost negligible (Fig. 2c). The width of the continental shelf determined biomass in Region 6 of the Canary and Region 1 of the Benguela Current. This is consistent with the advective control of both biomass and production in Region 6. In the Benguela region they were correlated also to the negative gradient, which implies an advective loss, but seen through ΔSST rather than transport. This region was the only one where production or biomass was driven by the negative gradient component.

The maximum correlation was between 0.32 and 0.9 for either biomass or primary production (Fig. 6). The absolute value of the correlation coefficient was less than 0.6 in eight regions for chlorophyll and in three for primary production. In some regions (four each in biomass and primary production) the correlation was comparable with more than one of the driving factors (Fig. 5). In the regions in which biomass or productivity were 'governed' by more than one factor, the continental shelf or PAR were often one of the additional factors. Table 5b summarizes the broader categories of environmental forcing. Large-scale circulation combined with local forcing and large-scale patterns were the dominant driving regimes for chlorophyll and primary production. PAR was very important, but it was associated with large-scale circulation in 75% of the cases for biomass.

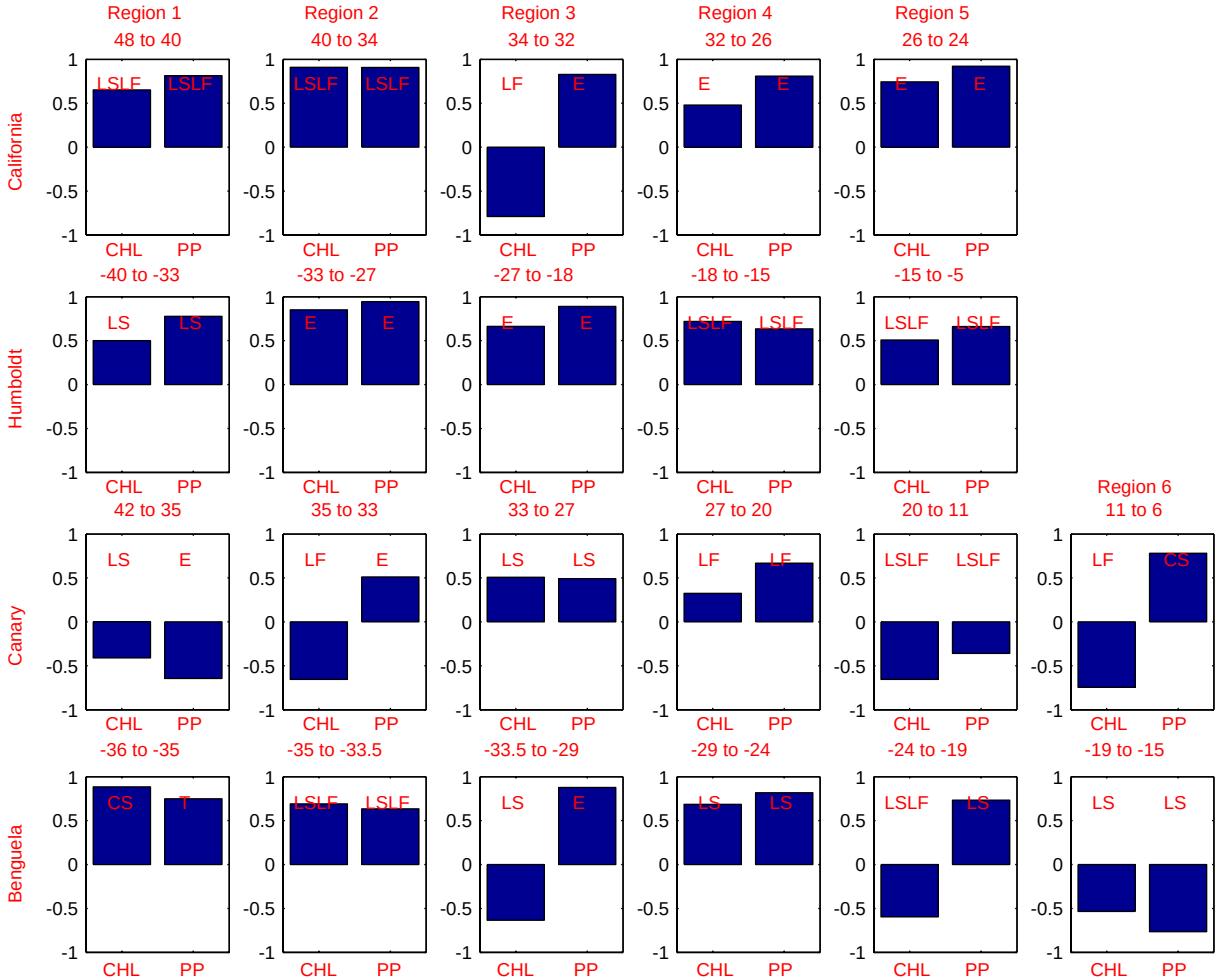

Fig. 6. Summary of the primary driving forces for biomass and primary production, the correlation coefficient and the environmental meaning. See Table 5 for more details.

Its strong relation with productivity is not surprising because production is estimated using PAR.

4. Discussion

4.1. Relationship between production regimes and maximum biomass and potential production

We estimated production regimes in an attempt to understand the seasonal and meridional patterns within each region. We do not show the results of analyses for the entire current because the variability of forcing between regions led both to small percentage of explained variance in the principal component analysis and to negligible correlations with the biological variables. The meridional structure of each EBC conditioned our definition of the regions. The fact that adjacent regions fall into different production regimes (Table 5a) supports our regional distinction.

Generally speaking, maximum values of peak biomass were observed in those regions in which the controlling component was related to large-scale forcing. There were eight regions with intermediate (3–6 mg Chl m^{-3}) peak chlorophyll concentrations and another eight with high values

(exceeding 6 mg Chl m^{-3}). In seven regions of each of these biomass categories, the biomass within that region was determined by either large-scale or the combination of large-scale and local forcing (Tables 2 and 5). The six regions of 'low' biomass (maxima of 3 mg Chl m^{-3} or less) were driven by local forcing or large-scale circulation. It is reasonable that maximum biomass will be reached when large-scale circulation and local forcing contribute in a similar fashion to the environmental variability. A negative relationship with local forcing (advective control) was seen in three regions of intermediate peak biomass and in one each of high and low chlorophyll maxima.

Potential production varied much less than biomass: eight of the regions had maximum primary production values between 3 and 4.5 g C m^{-2} day^{-1}, while seven were either above 4.5 g C m^{-2} day^{-1} or less than 3 g C m^2 day^{-1}. In all but five regions, the category of high biomass corresponded to that of high production. In three regions, high biomass was associated with intermediate production (Regions 1 and 2 of the California and Region 1 of the Peru-Humboldt). All three of these regions were driven by large scale or large scale and local forcing, and they presented peak transport values of about 0.4 m^2 s^{-1} in conjunction with significant seasonal variability in transport and PAR (Fig. 2, Tables 2 and 5). In two regions, intermediate biomass had high potential productivity: Region 5 of the Peru-Humboldt and Region 6 of the Benguela. Both were categorized as driven by large-scale forcing and PAR, and presented the two highest transport values (> 0.9 m^2 s^{-1}). Also in both cases PAR was high year-round due to the low latitude and peak biomass/production did not co-occur with the peak transport (in time in the case of the Peru-Humboldt and in space in the Benguela region). We propose that the seasonal cycle in PAR determined the observed divergence between biomass and production in these five regions.

4.2. Comparisons between all four EBCs

The only consistent relationship among the regional averages of the studied variables was between ΔSST and biomass (Fig. 7a). All four EBCs presented a linear relationship at an r of 0.6 if we eliminate the biomass values exceeding 8 mg Chl m^{-3} of the California, Peru-Humboldt, and Canary Currents (marked with crosses). The relationship derived for all four currents was a better descriptor for the Benguela Current

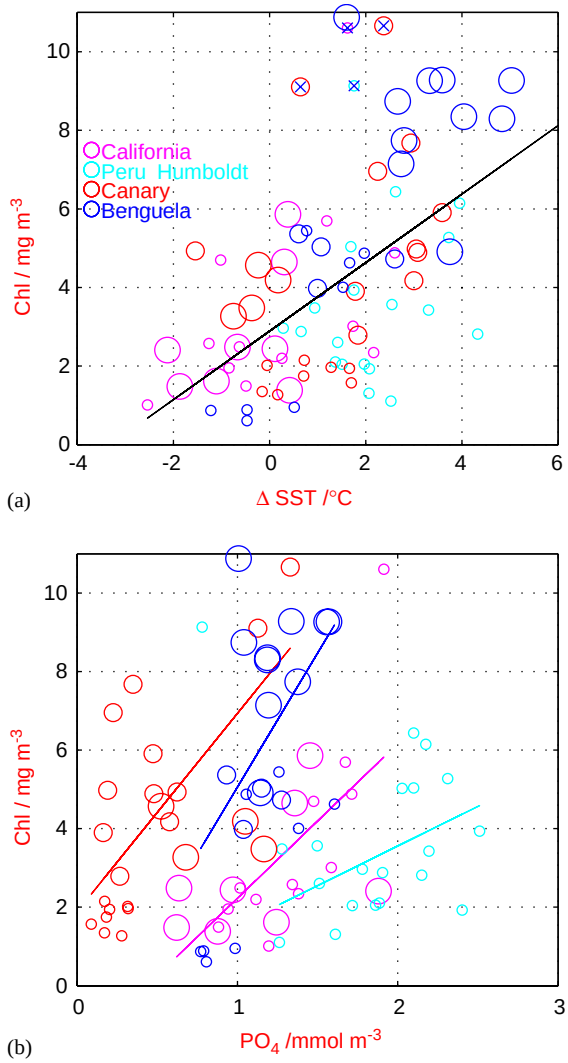

Fig. 7. Comparison of regional-averaged seasonal chlorophyll concentration for all four EBCs as a function of (a) ΔSST, and (b) PO_4. The California Current is denoted by magenta circles, the Peru-Humboldt by cyan, the Canary by red, and the Benguela by blue. The width of the outer shelf is indicated by circle size: the smaller circles represent ⩽80 km, the medium circles denote 80–120 km, and the largest circles represent > 120 km.

($r = 0.8$) than the other EBCs ($r > 0.4$). The Benguela/Peru-Humboldt Current had generally higher/lower biomasses for a given ΔSST than the relationship predicts. According to the linear relationship, an offshore temperature difference of zero corresponds to a biomass of 3 mg Chl m^{-3}. This value is an appropriate background level of phytoplankton concentration for the EBCs: the regional mean concentration of 40% of the regions is 3 mg Chl m^{-3} or less, while only 20% of the regions present $\Delta SST \leqslant 0°C$. It is interesting to note that those regions in which the width of the outer shelf is 80 km or less usually fell below the regression line, while those with shelf widths exceeding 120 km usually were above it. The intermediate shelf widths (80–120 km) were most scattered.

Fig. 7b shows the relationship between the PO_4 of the source water and the measured biomass, illustrating the differences between the nutrient supply in each EBC (nutrient content: Canary < Benguela ~ California < Peru-Humboldt) as well as the response of the planktonic ecosystem. Despite lower nutrient supply, the Atlantic EBCs 'supported' a higher concentration of phytoplankton (slopes ~6 mg Chl (mmol $PO_4)^{-1}$) than the Pacific EBCs (slopes ~3 mg Chl (mmol $PO_4)^{-1}$). The linear relationships drawn on the figure have correlation coefficients exceeding 0.66 in the California and Canary Currents and greater than 0.46 in the southern hemisphere. These observations are consistent with results of Minas et al. (1986) who found that nutrient utilization was much greater near 21°N in the Canary Current than at 15°S in the Peru-Humboldt. They proposed that grazing pressure nearshore at the latter site prevented optimal nutrient utilization.

The differences in nutrient utilization could also be due to the availability of iron (Fung et al., 2000). According to three maps of atmospheric dust deposition (Duce and Tindale, 1991; Tegen and Fung, 1995; Mahowald et al., 1999), the Canary Current region receives a large flux of dust from the Sahel and Saharan regions, while the California and Peru-Humboldt Currents present intermediate low-dust flux. The magnitude of the aeolian supply of dust to the Benguela Current is by contrast poorly established and is classified as either low (Duce and Tindale, 1991) or very high (Mahowald et al., 1999). In the California Current, varying levels of iron limitation have been identified (Hutchins et al., 1998). Possible sources of iron include benthic and riverine supply, as well as aeolian deposition from Asian events or Santa Ana winds in the southern California coast. In the Peru-Humboldt Current the most likely source of iron is benthic supply.

The width of the outer shelf (depicted by circle size in Fig. 7b) can be considered a proxy for benthic availability of iron. The lowest biomass for a given PO_4 concentration was in the Peru-Humboldt Current where the regionally averaged width of the outer shelf is always less than 80 km. In contrast, the Canary Current, which due to aeolian deposition should not require iron supply from depth, did not present a clear trend of biomass with shelf width. The lowest chlorophyll concentrations of the Canary Current (north of 32°N) coincide with the narrowest shelf width and are likely out of the influence of the atmospheric pathways of dust transport. There was not a strong relationship between width of the shelf and biomass in the California Current, although narrow shelves were usually found along or below the regression line. The Benguela Current had higher chlorophyll concentrations in wide shelf regions than in narrower ones, which may be related to benthic supply of iron or to biomass retention. It is not clear whether the apparent difference in biomass supported by available nutrients is due to differences in the efficiency of the phytoplankton community, perhaps related to the availability of iron, or to grazing pressure. An analysis of nutrient consumption patterns will be examined in conjunction with satellite estimations of biomass and production in a future study.

5. Conclusions

- All four EBCs presented high chlorophyll concentrations in the coastal region (> 2 mg Chl m^{-3}) and potential productivity exceeded 3 g C m^{-2} day^{-1} in 80% of the regions.
- Environmental variability within regions was determined primarily (30–60% of explained

variance) by large-scale circulation patterns (55% of regions), local forcing (18%), and large-scale circulation acting in concert with local forcing (27%).

- The meridional and seasonal patterns of biomass and potential productivity within each region were governed primarily by large-scale circulation (41% of regions), the combination of large scale and local forcing (32%), and local forcing alone (23%).
- Maximum biomass and primary production were observed in regions in which the local variability is dominated by large-scale circulation or the combination of large-scale and local forcing.
- The biomass sustained by the available nutrients in the Atlantic EBCs was twice as large as that of the Pacific EBCs for a given nutrient concentration. This apparent greater efficiency may be due to availability of iron, biomass retention, or differences in community structure.

Acknowledgements

We thank Darek Bogucki and three anonymous reviewers for valuable comments which improved the manuscript. We are grateful to CERSAT for the ERS-2 monthly files, the Goddard DAAC and the SeaWiFS Science Project for the SeaWiFS data set, the NOAA/NASA AVHRR Pathfinder project for SST via the JPL-PODAAC. Funding was provided by the NASA Ocean Biogeochemistry Program within the JGOFS Synthesis and Modeling Project. The research described in this paper was carried out at the Jet Propulsion Laboratory, California Institute of Technology, under a contract with the National Aeronautics and Space Administration.

References

Allen, J.S., 1973. Upwelling and coastal jets in a continuously stratified ocean. Journal of Physical Oceanography 3, 245–257.

Andrews, W., Hutchings, L., 1980. Upwelling in the southern Benguela Current. Progress in Oceanography 9, 1–81.

Bailey, G.W., 1985. Distribution and cycling of nutrients at four sites in the Benguela system. In: International Symposium on Upwelling in West Africa, Vol. 1, Instituto de Investigaciones Pesqueras, Barcelona, pp. 305–317.

Bakun, A., Nelson, C.S., 1991. The seasonal cycle of wind stress curl in subtropical Eastern Boundary Current regions. Journal of Physical Oceanography 21, 1815–1834.

Bernal, P.A., McGowan, J.A., 1981. Advection and upwelling in the California Current. In: Richards, F.A. (Ed.), Coastal Upwelling. American Geophysical Union, Washington, D.C., USA, pp. 381–399.

Blanco, J.L., Thomas, A., Carr, M.-E., Strub, P.T., 2001. Seasonal climatology of hydrographic conditions in the upwelling region off northern Chile. Journal of Geophysical Research 106, 11451–11467.

Calvert, S., Price, N.B., 1971. Upwelling and nutrient regeneration in the Benguela Current, October 1968. Deep-Sea Research 18, 505–523.

Campbell, J., Antoine, D., Armstrong, R., Balch, W., Barber, R., Beherenfeld, M., Bidigare, R., Bishop, J., Carr, M.-E., Esaias, W., Falkowski, P., Hoepffner, N., Iverson, R., Kiefer, D., Lohrenz, S., Marra, J., Morel, A., Ryan, J., Vedernikov, V., Waters, K., Yentsch, C., Yoder, J., 2002. Comparison of algorithms for estimating ocean primary production from surface chlorophyll, temperature, and irradiance. Global Biogeochemical Cycles 16 (3), 10.1029/2002GL015068.

Carr, M.-E., 2002. Estimation of potential productivity in Eastern Boundary Currents using remote sensing. Deep-Sea Research II 49, 59–80.

Carr, M.-E., Friedrichs, M., 2002. Primary production algorithm round-robin 3 (PPARR3): early results. Eos. Transactions American Geophysical Union, Vol. 83 (4), Ocean Sciences Meeting Suppl, Abstract OS12J-10, pp. 68.

Castro, C.G., Chávez, F.P., Collins, C.A., 2001. Role of the California undercurrent in the export of denitrified waters from the eastern tropical North Pacific. Global Biogeochemical Cycles 15 (4), 819–830.

Codispoti, L.A., Friedrich, G.E., 1978. Local and mesoscale influences on nutrient variability in the northwest African upwelling region near Cabo Corbeiro. Deep-Sea Research 25, 751–770.

Cushing, D.H., 1969. Upwelling and fish production. FAO Fisheries Technical Papers 84, 1–40.

Duce, R., Tindale, N., 1991. Atmospheric transport of iron and its deposition in the ocean. Limnology and Oceanography 36, 1715–1726.

FAO, 1999. The state of world fisheries and aquaculture 1998. FAO Documentation Group, Rome, Italy.

Fraga, F., Barton, E.D., Llinás, O., 1985. The concentration of nutrient salts in 'pure' North and South Atlantic Central Waters. In: International Symposium on Upwelling in West Africa, Vol. 1, Instituto de Investigaciones Pesqueras, Barcelona, pp. 25–36.

Friedrich, G.E., Codispoti, L., 1981. The effects of mixing and regeneration on the nutrient content of upwelling waters off peru. In: Richards, F.A. (Ed.), Coastal Upwelling.

American Geophysical Union, Washington, D.C., USA, pp. 221–227.

Fung, I., Meyn, S.K., Tegen, I., Doney, S., John, J., Bishop, J., 2000. Iron supply and demand in the upper ocean. Global Biogeochemical Cycles 14 (1), 281–295.

Gabric, A., Garcia, L., Van Camp, L., Nykjaer, L., Eifler, W., Schrimpf, W., 1993. Offshore export of shelf production in the Cape Blanc (Mauritania) giant filament as derived from Coastal Zone Color Scanner imagery. Journal of Geophysical Research 98 (3), 4697–4712.

Gill, A.E., 1982. Atmosphere-Ocean Dynamics. Academic Press, London.

Howard, K.L., Yoder, J.A., 1997. Contribution of the subtropical oceans to global primary production. In: Liu, C.-T. (Ed.), Space Remote Sensing of Subtropical Oceans, COSPAR Colloquia Series, Vol. 8, Proceedings of COSPAR Colloquium on Space remote sensing of subtropical oceans, Taiwan, Pergamon, New York, pp. 157–168.

Hutchins, D.A., DiTullio, G.R., Zhang, Y., Bruland, K.W., 1998. An iron limitation mosaic in the California upwelling regime. Limnology and Oceanography 43 (6), 1037–1054.

Jones, P.G.W., 1971. The southern Benguela Current region in February 1966: Part 1. chemical observations with particular reference to upwelling. Deep-Sea Research 18, 193–208.

Kearns, E.J., Carr, M.-E., 2003. Seasonal climatologies of nutrients and hydrographic properties on quasi-neutral surfaces for four coastal upwelling systems. Deep-Sea Research II, this issue (doi: 10.1016/j.dsr2.2003.07.014).

Lutjeharms, J., Shillington, F., Rae, C., 1991. Observations of extreme upwelling filaments in the southeast Atlantic Ocean. Science 235 (5021), 774–776.

Mahowald, N., Kohfeld, K., Hansson, M., Balkanski, Y., Harrison, S., Prentice, I., Schulz, M., Rodhe, H., 1999. Dust sources and deposition during the last glacial maximum and current climate: a comparison of odel results with paleodata from ice cores and marine sediments. Journal of Geophysical Research-Atmospheres 104, 15895–15916.

Minas, H.J., Minas, M., Packard, T.T., 1986. Productivity in upwelling systems deduced from hydrographic and chemical fields. Limnology and Oceanography 31, 1182–1206.

O'Toole, M.J., 1980. Seasonal distribution of temperature and salinity in the surface waters off in the southwest Africa, 1972–1974. Investigational Reports of the Sea Fisheries Research Institute of South Africa 121, 1–25.

Ryther, J.H., 1969. Photosynthesis and fish production in the sea. Science 166, 72–76.

Strub, P.T., Kosro, P.M., Huyer, A., 1991. The nature of cold filaments in the California Current system. Journal of Geophysical Research 96 (8), 14743–14768.

Tegen, I., Fung, I., 1995. Contribution to the atmospheric mineral aerosol load from land surface modification. Journal of Geophysical Research 100, 17726–18707.

Thomas, A.C., Carr, M.-E., Strub, P.T., 2001. Chlorophyll variability in Eastern Boundary Currents. Geophysical Research Letters 28 (18), 3421–3424.

Ware, D.M., 1992. Production characteristics of upwelling systems and the trophodynamic role of hake. In: Payne, A.I., Brink, K.H., Mann, K.H., Hillborn, R. (Eds.), Benguela Trophic Functioning, Sea Fisheries Research Institute, Cape Town, South Africa, Vol. 12, pp. 501–513.